Article

Discovery Medicine 2023; 35(176): 300–311
https://doi.org/10.24976/Discov.Med.202335176.31

An Exploration of Osteosarcoma Metastasis Diagnostic Markers Based on Tumor-Associated Neutrophils

Shan Tan[1], Rui Chao[2,*]

[1]Department of Orthopedics, The First Affiliated Hospital of Army Medical University, 400042 Chongqing, China
[2]Department of Orthopedics, Chongqing Emergency Medical Center, The Fourth People's Hospital of Chongqing, Chongqing University Central Hospital, 400014 Chongqing, China
*Correspondence: chaorui0910@sina.com (Rui Chao)
Published: 2 June 2023

Background: The high rate of the recurrence and metastasis of osteosarcoma (OS) is the major cause of its poor prognosis. There is a strong correlation between tumor-associated neutrophils (TANs) and tumor progression, progression, and metastasis. This study aimed to identify potential markers that could predict OS metastasis based on analysis of TANs in the tissues of OS patients.
Methods: A single-cell sequencing dataset (GSE152048), containing seven primary OS lesions, two recurrent OS lesions, and two lung metastatic OS lesions was used for TANs subset identification using the R software (version 4.1.0, R Project for Statistical Computing, Vienna, Austria; https://www.r-project.org/). Immune cell infiltration and immune score were analyzed using CIBERSORT algorithm and ESTIMATE database, respectively. The differentially expressed genes (DEGs) of TANs were used for weighted gene co-expression network analysis (WGCNA) to screen key genes associated with OS metastasis. Gene Ontology (GO) and Kyoto Encyclopedia of Genes and Genomes (KEGG) functional enrichment analysis were used to analyze the functions and signaling pathways involved in key genes. The mRNA levels of protein phosphatase 2 regulatory subunit B'gamma (*PPP2R5C*) were validated in human osteosarcoma cell lines U2-OS and MG63, human normal cervical endometrial cell line HUCEC, and human foreskin fibroblast (HFF-1) cell line by real-time qPCR (RT-qPCR). *PPP2R5C*-siRNA991 was transfected into U2-OS and MG63 for 48 h, then the expression levels of PPP2R5C, AKT serine/threonine kinase (*AKT*), and phospho-AKT (p-AKT) were determined by RT-qPCR and Western blotting. Cell proliferation, migration, and apoptosis were measured by cell counting kit-8 (CCK-8), Transwell, and flow cytometry, respectively.
Results: We identified TANs subsets in primary, metastatic, and recurrent OS. Immune infiltration analysis showed that TANs were expressed in OS. Compared with non-metastatic OS, metastatic OS had lower stromal score, immune score, ESTIMATE score, and higher tumor purity. WGCNA classified DEGs into five clusters, according to their function and identified *PPP2R5C*, protein phosphatase 2 regulatory subunit B'epsilon (*PPP2R5E*), tyrosine 3-monooxygenase/tryptophan 5-monooxygenase activation protein gamma (*YWHAG*) and CREB binding protein (*CREBBP*), as potential markers that may affect TANs-induced OS metastasis via hypoxia inducible factor 1 (HIF-1), phosphatidylinositol 3-kinases (PI3K)-AKT and Janus kinase (JAK)-signal transducers and activators of transcription (STAT) signaling pathways. *In vitro* experiments demonstrated that the mRNA and protein expressions of *PPP2R5C*, *PPP2R5E*, *YWHAG*, and *CREBBP* were highly expressed in U2-OS and MG63 cells ($p < 0.01$). Furthermore, *PPP2R5C* reduced proliferation and migration ($p < 0.01$) and increased apoptosis and p-AKT protein levels in U2-OS and MG6 cells ($p < 0.01$).
Conclusions: PPP2R5C affects OS metastasis via PI3K/AKT pathway, which may be a potential marker for OS metastasis and recurrence.

Keywords: osteosarcoma; metastasis; tumor-associated neutrophils; immune infiltration; *PPP2R5C*

Introduction

Osteosarcoma (OS), which occurs most commonly in the metaphysis, is the predominant bone tumor in children and adolescents. The prevalence of OS in children and adolescents between 0 and 14 years of age is estimated to be 3.2 per 1,000,000, with a male-to-female ratio of approximately 1.4 to 1 [1,2]. OS is highly susceptible to early metastasis, with the most prevalent sites of metastasis to the lung parenchyma and distant skeletal sites. Patients with localized OS can achieve a 5-year survival rate of 60–70%, which indicates that many patients will have recurrence within 5 years. The long-term survival rate for patients who develop OS metastases is a mere 19–30% [3]. Therefore, a prediction model based on differentially expressed genes (DEGs) between metastatic and non-metastatic OS is important for the early diagnosis of OS metastasis and prediction of patient prognosis, which are of great clinical significance.

The study of the tumor microenvironment (TME) provides a new direction for the study of OS. TME consists of the combination of tumor cells, extracellular matrix, tumor-associated fibroblasts, infiltrating immune cells, and tumor neovascularization. The infiltrating immune cells in TME are significantly associated with poor prognosis in patients with tumor [4,5]. In addition to tumor-associated macrophages, tumor-associated neutrophils (TANs) have been found to infiltrate a variety of tumors [6,7]. It is believed that neutrophils, as part of innate immunity, inhibit the growth and development of tumors [8]. Moreover, there is growing evidence that tumor infiltration with TANs is associated with poor prognosis [9,10]. TANs can promote tumor development and metastasis. Additionally, the serine protease found in the granules of TANs can directly induce tumor cell proliferation and promote tumor growth [11].

In this study, we investigated the differences of TANs in tumor tissues between patients with primary OS and patients with metastatic OS by single-cell transcriptome analysis and weighted gene co-expression network analysis (WGCNA). In addition, we performed *in vitro* validation of the obtained potential marker genes to provide a reference for the diagnosis, treatment, and prognosis of OS.

Methods

Data Procession and Dimension Reduction and Clustering Analysis

Single-cell sequencing dataset (GSE152048) containing seven primary OS lesions, two recurrent OS lesions, and two lung metastatic OS lesions was downloaded from the GEO database (clinical information of the OS patients is presented in Table 1). Seurat package in the R software (version 4.1.0, R Project for Statistical Computing, Vienna, Austria; https://www.r-project.org/) was used to screen cells with the following criteria: 200–7500 gene number, mitochondrial gene ratio $<$20%, and hemoglobin gene ratio $<$5%. Then, we integrated the data from all samples and used the Harmony algorithm to correct batch effects. RunPCA function and RunTSNE function were used for cell dimension reduction clustering, making dims equal to the inflection point shown in the ElbowPlot function. Expression of labeled genes was viewed, and cell annotation was conducted.

Immune Cell Infiltration and Immune Score Analysis

CIBERSORT package (version 1.03, Stanford University, Stanford, California (CA), the United States of America (USA); https://cibersortx.stanford.edu/) was used to predict the infiltration of immune cells in the TARGET database (https://www.cancer.gov/ccg/research/genome-sequencing/target). p value < 0.05 was used to screen immune cells. R software was used to analyze the infiltration of various immune cells in OS, and the ggplot plug-in was used to graph the heatmap. ESTIMATE algorithm (https://bioinformatics.mdanderson.org/estimate/index.html) was then used to score the traits of OS, including stromal score, immune score, ESTIMATE score, and tumor purity. ESTIMATE algorithm was used for estimating stromal, immune, and ESTIMATE scores, as per a previous study [12]. Tumor purity was calculated by the following formula: Tumor purity = cos (0.6049872018 + 0.0001467884 $\times$ ESTIMATE score).

Differentially Expressed Genes (DEGs) Analysis

Wilcox rank sum test of the Seurat package (version 3.1.1, Paul Hoffman, Satija Lab and Collaborators, New York Genome Center, NY, USA) was used to screen DEGs in different cells. Genes expressed in more than 25% of cells in at least one comparison group were typically screened for differential expression when comparing one type of cell with all other types of cells, and this analysis was commenced with a different screening criterion of fold change $\geq$1.5 or $\leq$–1.5 and trend $<$0.1.

WGCNA Analysis

The RNA sequencing data from all samples were subjected to WGCNA analysis using the WGCNA package (version 1.7.0) in R software. The optimal soft threshold was calculated using the pickSoftThreshold function. The blockwiseModules function was used to construct the co-expression matrix. Principal component analysis (PCA) was performed on the genes within the modules, and principal component 1 was used as the module eigengenes (MEs). Modules closely related to OS metastasis were screened by calculating the correlation coefficient r and the corresponding p values.

Function and Pathway Enrichment Analysis

The Database for Annotation, Visualization and Integrated Discovery (DAVID) Bioinformatics Resources (https://david.ncifcrf.gov/) was used to analyze the main functions and signaling pathways of the screened DEGs and to explore their potential biological significance. Gene Ontology (GO) analysis was performed to investigate the specific molecular function, biological process, and cellular component of DEGs. Kyoto Encyclopedia of Genes and Genomes (KEGG) analysis was used to investigate the signaling pathways in which the DEGs are involved.

Protein-Protein Interaction (PPI) Network Analysis

PPI analysis of the screened DEGs was performed using the STRING database (https://cn.string-db.org/) to construct the interaction network. The constructed network was imported into Cytoscape software (version 3.8.0, The Cytoscape Consortium, San Diego, CA, USA; http://www.cytoscape.org/), and the MCC algorithm in the cytohubba plug-in was used to further screen the most closely related target genes.

Table 1. Basic clinical information of the OS patients (n = 11).

Sample	Age (years)	Sex (male/female)	Type	Necrosis rate
BC2	11–38	5/6	Primary	<90%
BC3			Primary	<90%
BC5			Primary	≥90%
BC6			Primary	≥90%
BC10			Metastasis (lung)	<90%
BC11			Recurrent	<90%
BC16			Primary	<90%
BC17			Metastasis (lung)	<90%
BC20			Recurrent	<90%
BC21			Primary	<90%
BC22			Primary	<90%

Cell Culture

Human osteosarcoma cell lines U2-OS (catalog #CL-0236) and MG63 (catalog #CL-0157), human normal cervical endometrial cell line HUCEC (catalog #CP-H059), and human foreskin fibroblast (HFF-1) cell line (catalog #CL-0352) were supplied by Procell (Wuhan, China). All cell lines were authenticated by Short Tandem Repeat (STR) Profiling and tested free of mycoplasma infection using Mycoplasma Detection Kit (catalog #CA1080, Solarbio, Beijing, China). U2-OS cells were cultured in McCoy's 5A (catalog #PM150710, Procell, Wuhan, China) supplemented with 10% fetal bovine serum (FBS; catalog #S1580, Biowest, Kansas City, Missouri (MO), USA) and 1% penicillin-streptomycin (P/S; catalog #15140122, Gibco, Thermo Fisher Scientific, Waltham, Massachusetts (MA), USA). MG-63 cells were cultured in minimum essential medium (MEM; catalog #PM150410, Procell, Wuhan, China), supplemented with 10% FBS and 1% P/S. HUCECs were cultured in 1640 medium (catalog #PM150110, Procell, Wuhan, China), including 10% FBS and 1% P/S. HFF-1 cells were cultured in Dulbecco's Modified Eagle medium (DMEM), containing 15% FBS and 1% penicillin/streptomycin. The cells were incubated in an incubator with 5% CO_2 and 95% O_2 air at 37 °C.

Cell Transfection

We referred to a previous study [13] for *PPP2R5C*-siRNA (991~1015nt) design. The sequences were as follows: sense, 5′-CAGUGGUGAUGGCACUUCUCAAAUA-3′; antisense, 5′-UAUUUGAGAAGUGCCAUCACCACUG-3′. The *PPP2R5C*-siRNA (40 nM) and Lipofectamine RNAiMAX (2 μL; catalog #13778030, Thermo Fisher Scientific, Waltham, MA, USA) were separately diluted in Opti-MEM (catalog #31985070, Gibco, Thermo Fisher Scientific, Waltham, MA, USA) with a volume of 25 μL. Then, the two solutions were mixed completely and allowed to stand at room temperature for 15 min. The 50 μL transfection mixture was added to the cells followed by incubation for 48 h.

Cell Counting Kit-8 (CCK-8) Assay

Cell proliferation rate was counted using a CCK-8 assay. The transfected cells were treated with CCK-8 solution (catalog #C0037, Beyotime, Shanghai, China) and incubated at 37 °C for 30 min. The absorbance was measured at 450 nm, using an FLx800 fluorescence microplate spectrophotometer (Bio-Tek Instruments, Winooski, Vermont, USA) to obtain the percentage of proliferating cells.

Transwell Migration Assay

The cells were serum-starved overnight. The cells at a density of 5×10^5 were then seeded onto the upper chamber and cultured in a serum-free medium. The cells seeded onto the lower chamber were cultured in DMEM supplemented with 10% FBS. After 18 hours of incubation, the non-migrated cells on the upper surface of the filter were wiped with a cotton swab. The cells that adhered to the lower surface were fixed with 70% methanol (catalog #M813895, Maclin Biochemical Technology Co., Ltd., Shanghai, China) and stained with 0.1% crystal violet (catalog #61135, Sigma Aldrich, St. Louis, MO, USA). Three fields were randomly counted for each well.

Cell Apoptosis Assay

The cells were fixed using the Fix&Perm Kit (catalog #GAS004, Invitrogen, Thermo Fisher Scientific, Waltham, MA, USA) for 15 min in a dark room. A Cell Apoptosis Kit was used for flow cytometry (catalog #V13242, Thermo Fisher, Waltham, MA, USA). The cells were incubated in 5 μL Annexin V (1:4 dilution) and 1 μL 100 μg/mL propidium iodide for 15 min. Then the cells were centrifuged and resuspended in phosphate-buffered saline (PBS; catalog #P1022, Solarbio, Beijing, China) and centrifuged. The cells were incubated with Annexin-binding buffer in the dark at 4 °C for 1 h. After repeated centrifugation and resuspension, the cells were transferred into flow tubes and apoptosis measured using the CytoFLEX flow cytometry (Beckman Coulter, Brea, CA, USA).

Real-Time qPCR (RT-qPCR)

Total RNA of the cells was isolated using the TRIzol reagent (catalog #15596026, Invitrogen, Thermo Fisher Scientific, Waltham, MA, USA). The cDNA was synthesized using the RNA reverse transcription kit (catalog #RR036A, Takara, Shiga, Japan). RT-qPCR was then performed using the One-step RT-PCR kit (QIAGEN, Valencia, CA, USA) on an ABI 7300 Real-time instrument (Applied Biosystems, Foster City, CA, USA). The reaction was conducted at a total volume of 50 μL containing 10 μL of 5$\times$ OneStep RT-PCR buffer, 2 μL of dNTP mix, 2 μL of OneStep RT-PCR enzyme mix, 600 nM of each primer, and 5 μL of template. Optimized amplification conditions were: 50 °C for 30 min, followed by 15 min at 95 °C, and 40 cycles of 15 sec at 30 s at 94 °C, 30 s at 55 °C and 1 min at 72 °C, and 10 min for 72 °C. Primers for RT-qPCR were: *PPP2R5C*: forward, ACACAGTAGAATCAGAGGGAACA, reverse, AAGAGGACGCAACACTGACG; *PPP2R5E*: forward, TAGCCCCCATTTTCAGGTGG, reverse, GCTCGTCAAACATGGTGCTG; *YWHAG*: forward, CCTGGAGGGTCATCAGTAGC, reverse, ACGCACGGACCATCTCAATC; *CREBBP*: forward, CTGAGAACTTGCTGGACGGA, reverse, TTGATACTAGAGCCGCTGCC; *AKT*: forward, GCACAAACGAGGGGAGTACA, reverse, AAGGTGCGTTCGATGACAGT; Glyceraldehyde-3-phosphate dehydrogenase (*GAPDH*): forward, GCCACCCAGAAGACTGTGGAT, reverse, AAGGCCATGCCAGTGAGC. Relative gene expression levels were determined by the $2^{-\Delta\Delta Ct}$ method. GAPDH, the internal standard, was used to normalize gene expression.

Western Blotting

Cell protein was isolated using the Protein Extraction Reagent (Thermo Fisher Scientific, Waltham, MA, USA) and quantified using the BCA Protein Assay Kit (Thermo Fisher Scientific, Waltham, MA, USA). Then, the protein (20 μg) was subjected to 12% SDS-PAGE and transferred onto a nitrocellulose membrane. After the membrane was blocked in 5% bovine serum albumin (BSA), the membrane was incubated with primary antibody overnight at 4 °C. The primary antibodies were: PPP2R5C (catalog #A5480, 1:800), PPP2R5E (catalog #A15084, 1:800), YWHAG (catalog #A18060, 1:1100), CREBBP (catalog #A1334, 1:1000), AKT (catalog #A11016, 1:1000), p-AKT (catalog #AP0637, 1:1000), and GAPDH (catalog #A19056, 1:500) (all from ABconal, Wuhan, China). After washing the membranes with PBS, they were incubated with secondary antibody Goat Anti-Rabbit IgG (catalog #AS014, 1:4000, ABconal, Wuhan, China) for 1 h at 25 °C. The bands were visualized, using the Novex chemiluminescent substrates (catalog #WP20005, Invitrogen, Thermo Fisher Scientific, Waltham, MA, USA) in a Tanon 6600 system (Tanon Technology, Shanghai, China). The grey value was measured using ImageJ image software (version 1.44p, National Institutes of Health, Bethesda, Maryland, USA). Relative protein expression (standardized to GAPDH) was quantified based on the grey values.

Statistical Analysis

DEGs in the single-cell sequencing data were determined using a two-sided Wilcoxon rank sum test. The experimental data were analyzed using GraphPad Prism (version 9.0, GraphPad Software, San Diego, CA, USA). Data are presented as mean $\pm$ standard deviation. All results were obtained from at least three independent experiments. A one-way ANOVA followed by post hoc test was used for multiple groups comparison. p value < 0.05 was considered significant.

Results

Identification of TANs Subsets

We identified 26 cell subsets from 100,987 single cells by screening, dimension reduction and clustering, and annotation (Fig. 1A). Cell subsets 0, 9, and 18 showed high expression levels of the myeloid cell marker genes *CD74*, *CD14*, and *FCGR3A* (Fig. 1B). Then, cluster analysis was further conducted on these three subsets, and a total of 15 clusters were obtained; the cluster expressing TANs marker genes *S100AB* and *G0S2* was mainly in subset 8 [14] (Fig. 1C). This subset consisted of TANs. Therefore, WGCNA analysis was conducted on their DEGs. TANs infiltration was observed in both metastatic and recurrent OS, but the number of infiltrating cells was less than that of primary OS (Fig. 1D).

Immune Cell Infiltration and Immune Score

TARGET transcriptome data were analyzed to determine the degree of immune cell infiltration in tissues with OS. In general, TANs had a high proportion in OS among the 22 immune cell classifications, second only to follicular T-helper cells (Fig. 2A). Additionally, we compared the immune environment in metastatic and non-metastatic OS with the ESTIMATE algorithm. The results showed that the stromal score, immune score, and estimate score in metastatic OS were lower than non-metastatic OS, while tumor purity in metastatic OS was higher than non-metastatic OS (Fig. 2B). The scoring of each sample is provided in **Supplementary Table 1**.

Key Module Screening

The WGCNA package of the R software determined that the soft threshold β was 4 and the mean connectivity was close to 0 (Fig. 3A). DEGs from TANs subsets with similar biological functions were grouped into one module after dynamic cutting. There were six modules obtained. DEGs in the gray module were unrelated to any other module (Fig. 3B). Correlation and significance analyses were

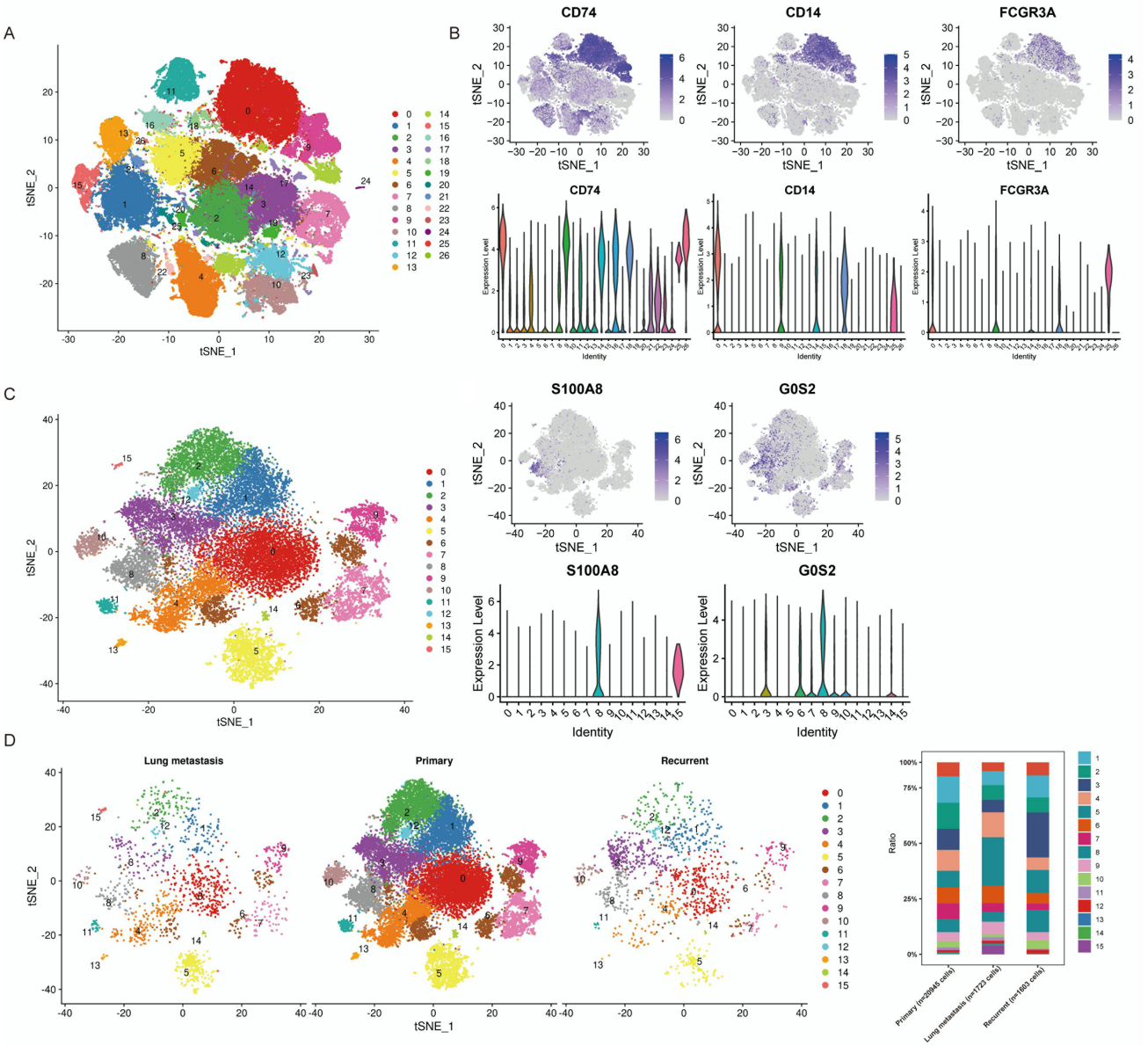

Fig. 1. Identification of myeloid cells and TANs from 7 primary OS, 2 recurrent OS, and 2 lung metastatic OS and analyzed using the RunPCA function and the RunTSNE function in the R software. Visualization was performed using t-SNE algorithm in the Seurat package. (A) A total of 26 cell clusters were identified. Different colors represent different cell clusters. (B) Myeloid cells were distributed in subsets 0, 9, and 18 by analyzing the expression of marker genes *CD74*, *CD14*, and *FCGR3A*. (C) TANs distribution in subset 8 was analyzed by the expression of marker genes *S100A8* and *G0S2*. (D) TANs (subset 8) distribution in primary OS, metastatic lung cancer, and recurrent OS. Primary OS had the largest number of TANs infiltration.

performed to determine the relationship between each module and OS metastasis. The results showed that the brown module (r coefficient = 0.25, p value = 0.02) was more correlated with OS metastasis than the other modules. Therefore, DEGs in brown module might have an important impact on OS metastasis.

Functional Enrichment Analysis of DEGs

GO analysis showed that most DEGs in the brown module participated in cell components, such as cell-substrate junction, focal adhesion, cytoplasmic ribonucleoprotein granule, and ribonucleoprotein granule (Fig. 4), suggesting that these DEGs might promote OS metastasis to other organs and distant bones by affecting the composition of cell matrix. The DEGs in the brown module were functionally clustered into five clusters with the MCODE plug-in of Cytoscape; they were found to participate in the functions of the cell components mentioned above (Fig. 5A). In addition, KEGG analysis showed that signaling pathways involved in DEGs were mainly related to HIF-1, PI3K-AKT, and JAK-STAT (Fig. 5B). We, therefore, spec-

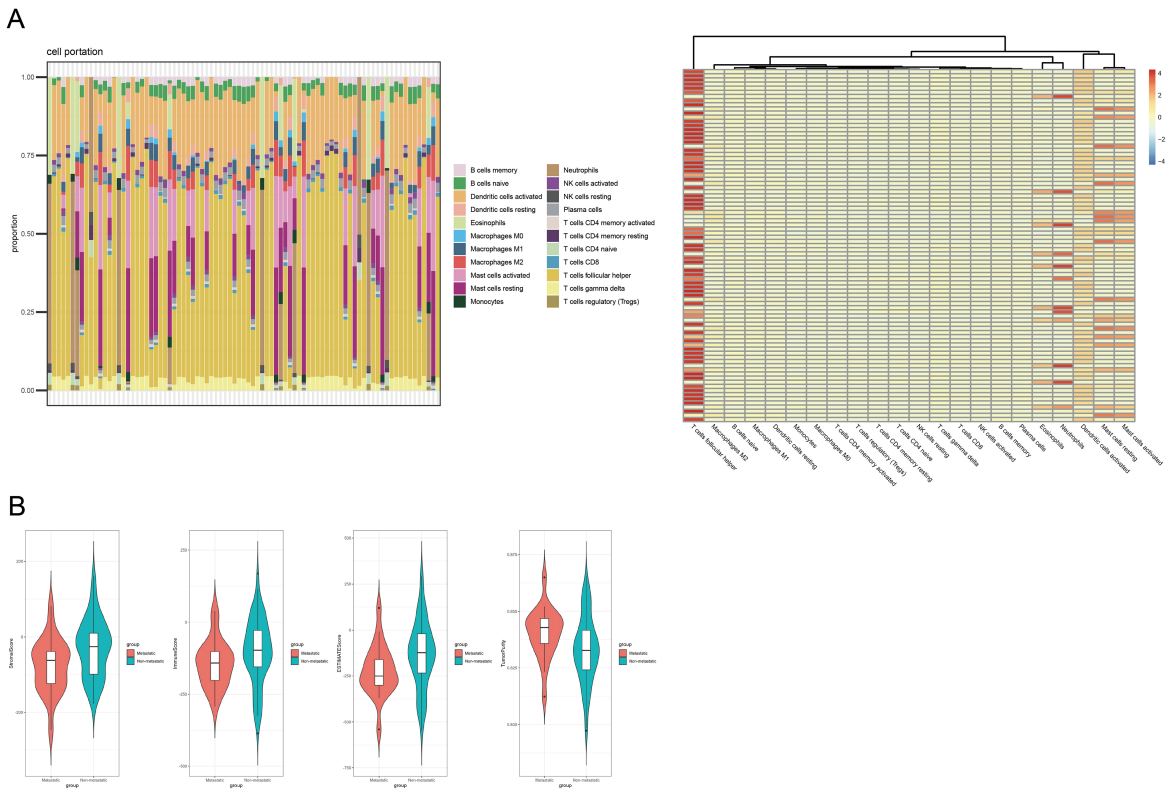

Fig. 2. Immune cell infiltration and immune score in OS cells. (A) Immune cell infiltration was analyzed using the CIBERSORT algorithm. TANs had a high percentage of TANs infiltration, second only to T follicular helper cells. (B) ESTIMATE database was used to analyze the stromal score, immune score, ESTIMA score, and tumor purity between metastatic OS and non-metastatic OS.

ulated that differential expression of *PPP2R5C*, *PPP2R5E*, *YWHAG*, and *CREBBP* in TANs between metastatic OS and non-metastatic OS affected OS metastasis.

Determination of PPP2R5C, PPP2R5E, YWHAG, and CREBBP in Human OS Cell Lines

To prove our hypothesis, we determined whether *PPP2R5C*, *PPP2R5E*, *YWHAG*, and *CREBBP* are expressed in the human OS cell lines and normal cell lines. As presented in Fig. 6A,B, the relative mRNA and protein levels of *PPP2R5C*, *PPP2R5E*, *YWHAG*, and *CREBBP* were high in human OS cell lines U2-OS and MG63 ($p < 0.01$), whereas much lower levels were observed in the normal cell lines HUCEC and HFF-1. Furthermore, the relative mRNA and protein levels of *PPP2R5C*, *PPP2R5E*, *YWHAG*, and *CREBBP* were not significantly different between U2-OS and MG63 cells ($p > 0.05$). However, their levels in HUCEC and HFF-1 cells were significantly decreased compared with U2-OS and MG63 cells ($p < 0.01$).

Effect of PPP2R5C Interference on Human Osteosarcoma Cell Lines

PPP2R5C, *PPP2R5E*, *YWHAG*, and *CREBBP* were found to be involved in OS metastasis via HIF-1, PI3K-AKT, and JAK-STAT signaling pathways. We speculated that *PPP2R5C* activated the AKT/STAT signaling through phosphorylation of related proteins, leading to higher proliferating and migrating ability of tumor cells. After siRNA991 was transfected into the U2-OS and MG63 cells, the *PPP2R5C* mRNA and protein expression levels in both cell lines decreased significantly ($p < 0.01$) (Fig. 7A,B). We then determined the signaling activity of the PI3K/AKT pathway in both U2-OS and MG63 cells. After transfection with *PPP2R5C*-siRNA, the relative mRNA and protein levels of *PPP2R5C* in both cells were significantly decreased compared with the non-transfected group or vector-transfected group ($p < 0.01$). The AKT mRNA level was not affected by *PPP2R5C*-siRNA transfection ($p > 0.05$), while the phospho-AKT (p-AKT) protein levels in the *PPP2R5C*-siRNA transfected group were significantly decreased compared with the non-transfected or vector transfected groups ($p < 0.01$) (Fig. 7A,B).

Inhibition of *PPP2R5C* expression and PI3K/AKT signaling also affected the characteristics of the cancer cells. After *PPP2R5C*-siRNA treatment, the cell viability (Fig. 8A) and migration ability (Fig. 8B) were significantly reduced, whereas the apoptosis rates were significantly increased in both cell lines (Fig. 8C). These results suggest that *PPP2R5C* may be a potential marker for metastasis and recurrence of OS.

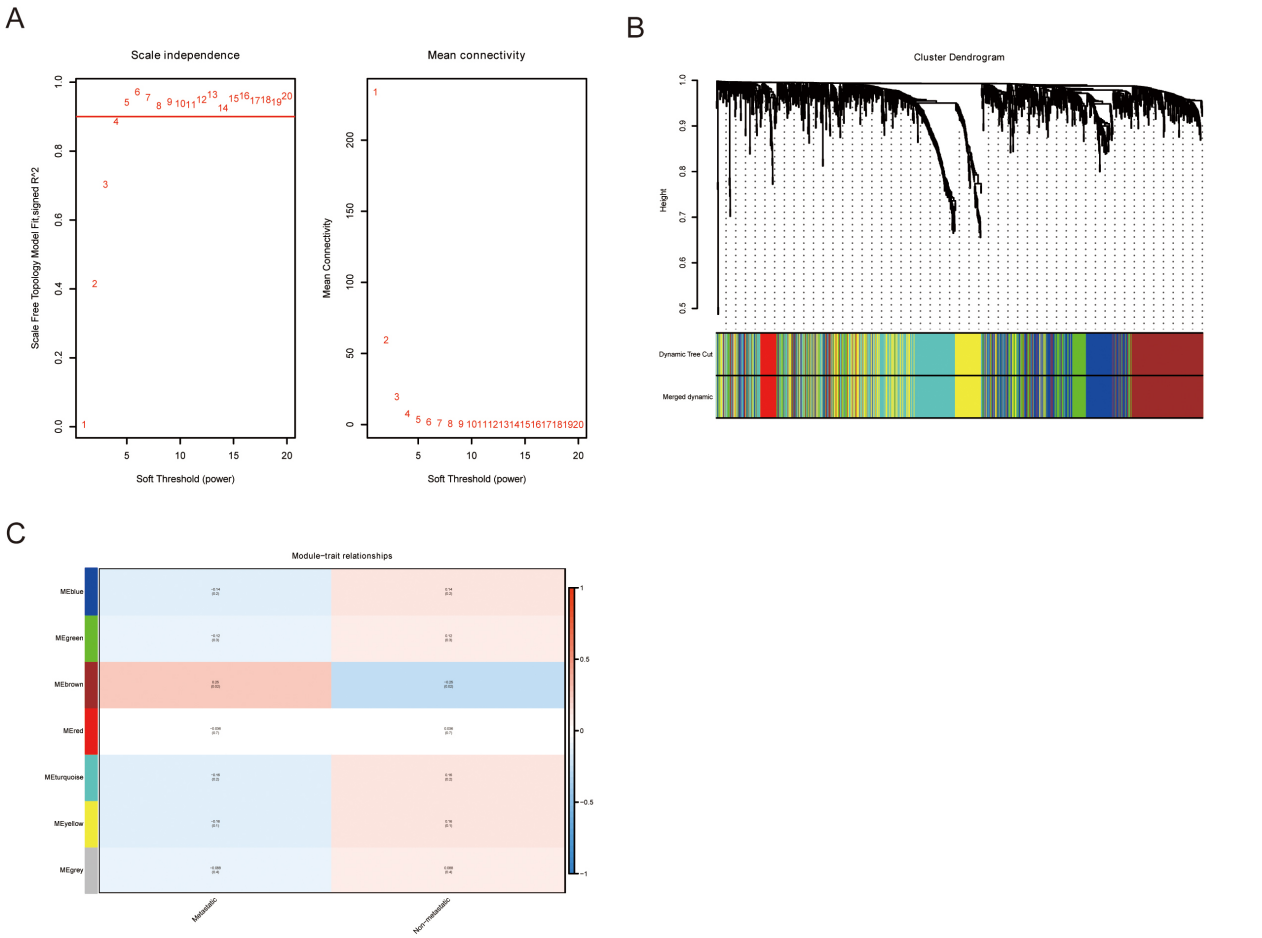

Fig. 3. Co-expression network module of DEGs construction by WGCNA. (A) Soft threshold was determined by calculating scale independence and mean connectivity. (B) Gene clustering tree and module cutting were used to group DEGs with similar biological functions into the same co-expression module, and each module was assigned a different color. (C) Module related to OS metastasis was screened by analyzing the relationship between modules and traits.

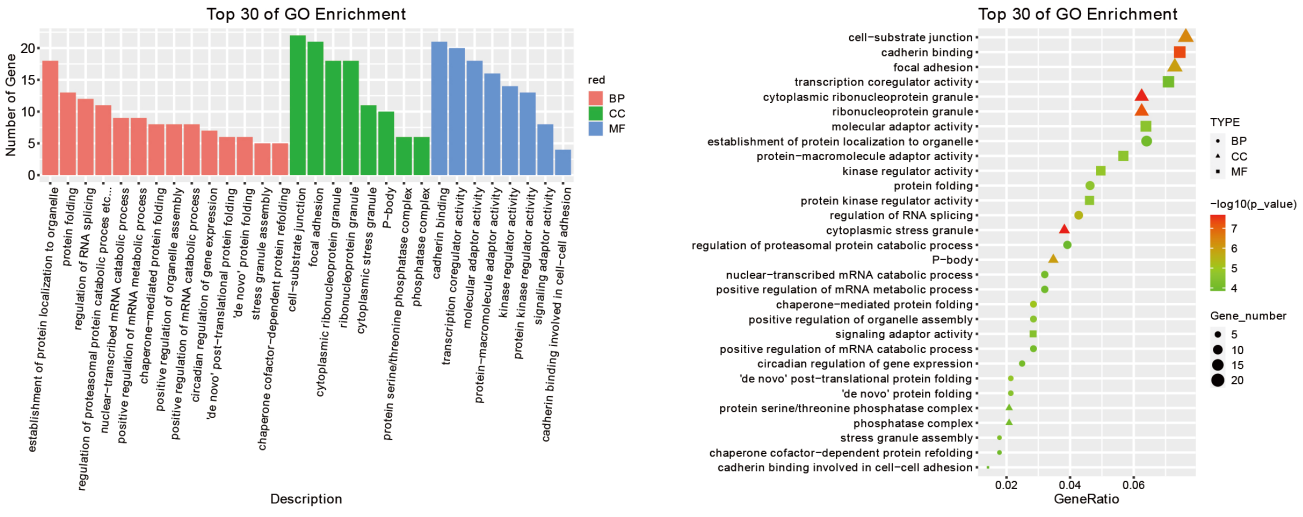

Fig. 4. GO enrichment analysis was performed on DEGs by DAVID database. The top 30 items were generated by calculating the number of genes and *p* value of each item. Each gene may be involved in BP (biological processes), CC (cell components), and MF (molecular functions).

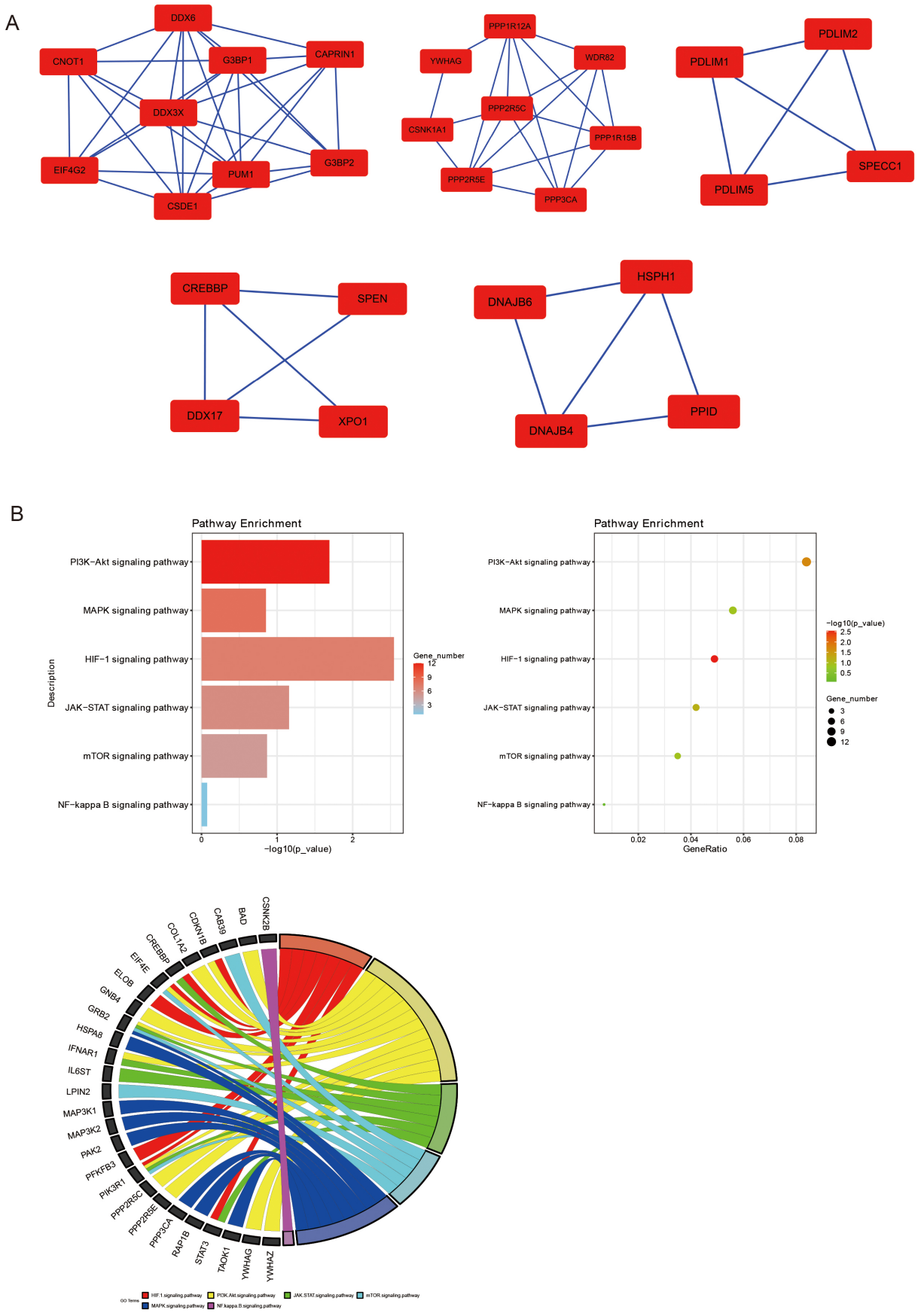

Fig. 5. Functional clustering and KEGG enrichment analysis of the DEGs. (A) DEGs were categorized into 5 clusters according to functional and Cytohubba scores. (B) The signaling pathways of the DEGs were presented by ranking the *p* values.

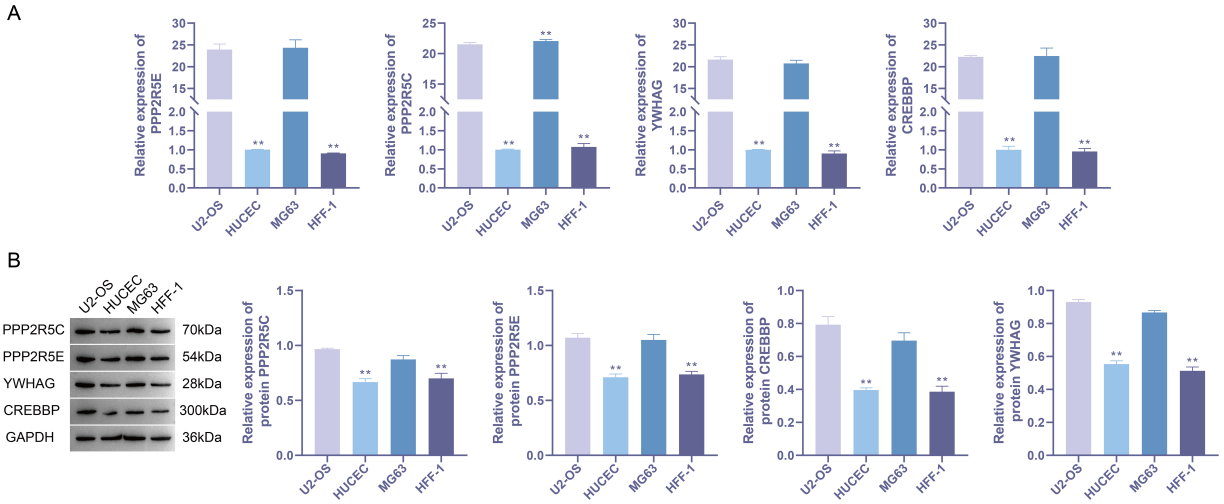

Fig. 6. RT-qPCR and Western blotting were used to determine the levels of *PPP2R5C*, *PPP2R5E*, *YWHAG*, and *CREBBP* in non-treated U2-OS, MG63, HUCEC, and HFF-1 cells. (A) The mRNA levels of *PPP2R5C*, *PPP2R5E*, *YWHAG*, and *CREBBP* were determined by RT-qPCR (n = 3 per group). (B) The protein levels of PPP2R5C, PPP2R5E, YWHAG, and CREBBP were determined by Western blotting (n = 3 per group). A one-way ANOVA followed by post hoc test was used for multiple groups comparison. ** $p <$ 0.01 vs. U2-OS.

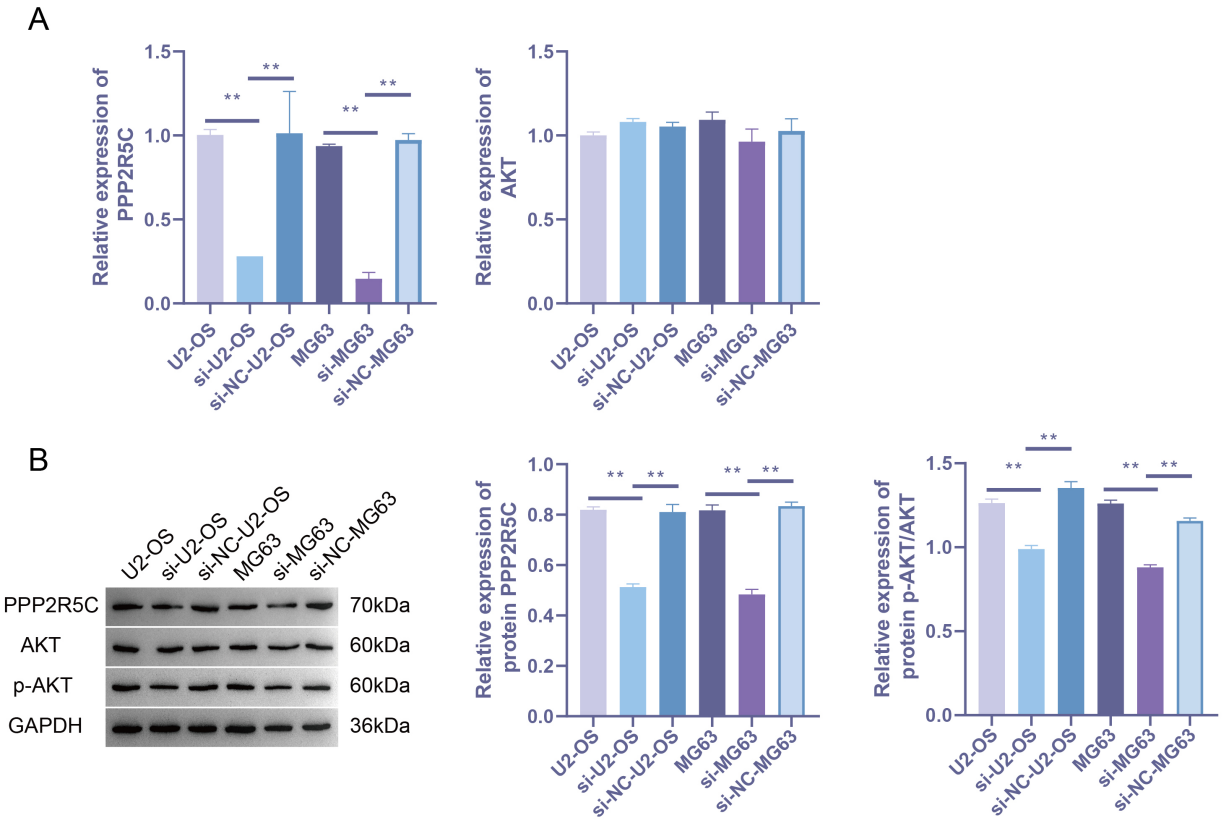

Fig. 7. RT-qPCR and Western blotting assays used to determine the levels of *PPP2R5C*, *AKT*, and p-AKT in U2-OS and MG63 cells 48 h after siRNA999 transfection. (A) The mRNA levels of *PPP2R5C* and *AKT* were determined by RT-qPCR (n = 3 per group). (B) The protein levels of PPP2R5C, AKT, and p-AKT were determined by Western blotting. A quantitative analysis of the p-AKT/AKT ratio was used as an indicator of phosphorylation (n = 3 per group). A one-way ANOVA followed by post hoc test was used for multiple groups comparison. ** $p <$ 0.01.

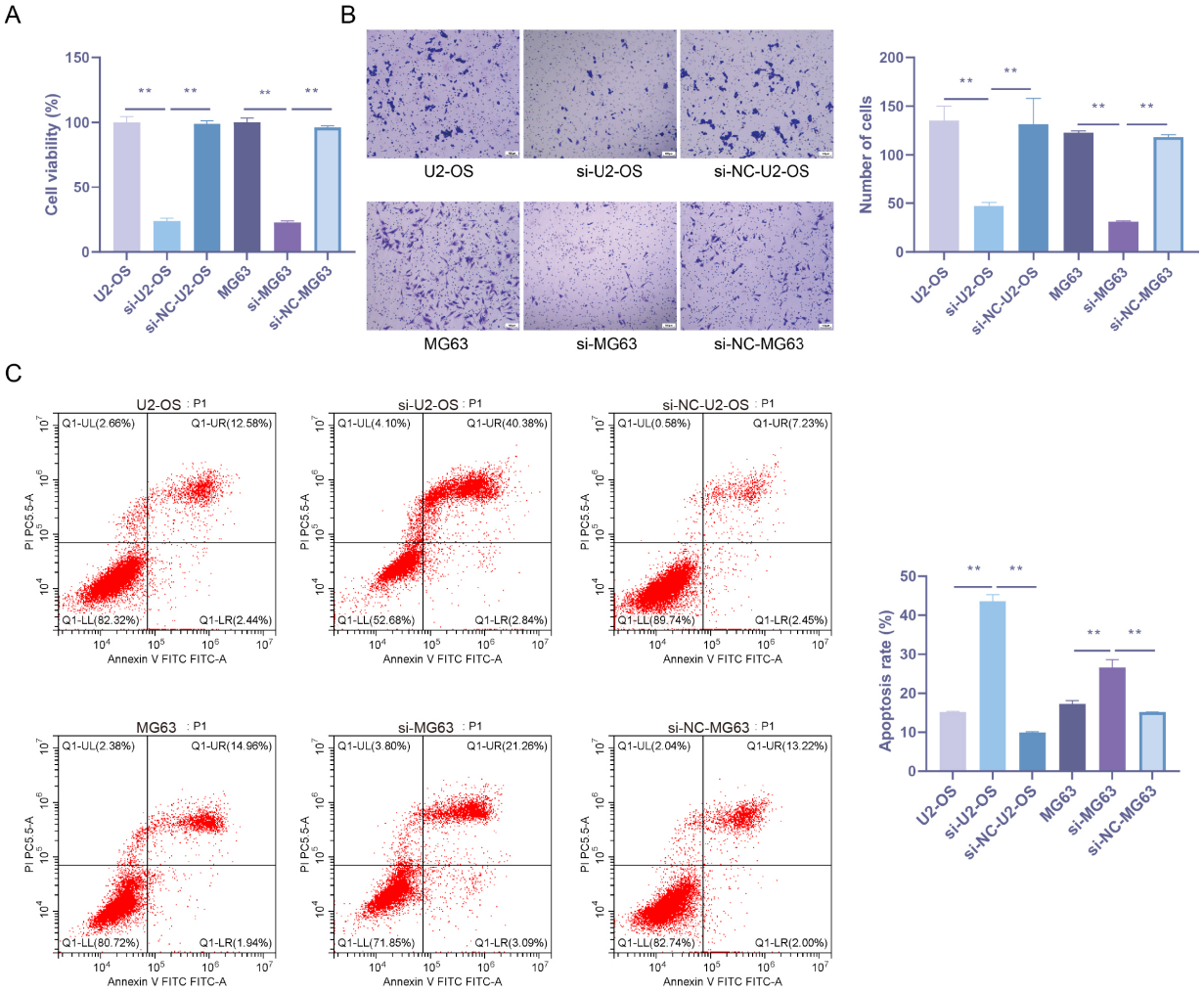

Fig. 8. The cell viability, migration rate, and apoptosis rate were measured in U2-OS and MG63 cells 48 h after siRNA999 transfection by CCK-8 assay, Transwell assay, and flow cytometry, respectively. (A) CCK-8 assay was used to determine cell viability of U2-OS and MG63 cells (n = 3 per group). (B) Transwell assay was used to determine the migration rate of U2-OS and MG63 cells (n = 3 per group). Scale bar = 100 μm. (C) Flow cytometry was used to quantify the apoptosis rate (n = 3 per group). A one-way ANOVA followed by post hoc test was used for multiple groups comparison. ** $p < 0.01$.

Discussion

TANs are similar to tumor-associated macrophages and are classified into N1 and N2 phenotypes, based on their anti- or pro-tumor properties [15]. Studies have shown that TANs play an important role in tumor metastasis. In breast cancer, TANs not only contribute to lung metastasis but also accumulate in the lung, before the metastasis of breast cancer cells to the lung, providing a suitable tumor microenvironment for metastasis of cancer cells [10,16]. As the tumor progresses, intratumor TANs gradually change from N1 to N2 in mice with lung cancer [17]. It is believed that the increase in tumor cell proliferation and invasion induced by N2 phenotype TANs is associated with granulocyte elastase and matrix metalloproteinase-9 (MMP9). The elastase is secreted into tumor cells by TANs, interacts with insulin receptor substrate-1, and degrades, resulting in the activation of PI3K to promote the phosphorylation of AKT, thus activating the PI3K/AKT signaling pathway to promote the proliferation and survival of tumor cells [18]. TANs are the main sources of MMP9; angiogenesis is induced and tumor growth is promoted by matrix MMP9 activating downstream vascular endothelial growth factor and fibroblast growth factor [19]. In this study, the single-cell sequencing data revealed that TANs are expressed in a high proportion in immune infiltrating cells of OS. ESTIMATE analysis found that patients with metastatic OS had a lower stromal score and immune score and higher ESTIMATE score and tumor purity than those with non-metastatic OS. These results suggest that a poor prognosis is associated with metastatic OS due to the presence of more tumor cells in the tissue, fewer immune cells, and lower immune activity. Furthermore, data mining of DEGs using WGCNA revealed significant differences in the expressions

of *PPP2R5C*, *PPP2R5E*, *YWHAG*, and *CREBBP* genes in TANs between metastatic OS and non-metastatic OS. Additionally, these key genes may act via the HIF-1, PI3K-AKT, and JAK-STAT signaling pathways.

We then used U2-OS and MG63 cells for *in vitro* validation. *PPP2R5C* expression was significantly increased in OS cells, consistent with previous studies. After inhibiting the *PPP2R5C* expression with siRNA991, the PI3K-AKT pathway was activated, the proliferation and migration of the cancer cells were suppressed, and cell apoptosis was increased. These results demonstrated the promotive function of *PPP2R5C* in OS metastasis. *PPP2R5C* and *PPP2R5E* are subunits of protein phosphatase 2A (PP2A). PP2A is one of the four major serine/threonine phosphatases involved in the negative regulation of cell growth and differentiation [20]. *PPP2R5C* can inhibit apoptosis in skeletal and cardiac muscle [21], suppress uncontrolled cell growth by blocking cell cycle and regulating telomerase activity, and reduce MMP1 transcription by blocking Raf, MEKl/2, and ERKl/ERK2 signaling pathways [22]. A previous study showed that *PPP2R5C* was increased significantly in patients with acute myeloid leukemia compared with healthy controls, suggesting an important relationship between *PPP2R5C* and tumor development [23]. In addition, it has been shown that decreasing the expression of *PPP2R5E* in brain tissue reduces the risk of non-small cell lung cancer and bladder cancer [24,25]. *YWHAG* belongs to the YWHA protein family, whose members participate in cell cycle and apoptosis [26]. Studies have shown that *YWHAG* is overexpressed in breast cancer and pancreatic cancer, which may potentially be a prognostic marker [27,28]. In advanced lung cancer, *YWHAG* down-regulates p53 expression, resulting in uncontrolled cell proliferation [29]. *YWHAG* is also associated with metastasis of cancer cells. The ability of breast cancer cells to invade and metastasize is enhanced when *YWHAG* is present during epithelial mesenchymal transition [30]. *CREBBP* also has the potential as a cancer prediction target [31]. A variety of disordered trans-active domains interact with *CREBBP* through its various domains, including p53, hypoxia-inducible factor 1α, NF-κB, and STAT proteins, which counteract cytokines by competing with disordered viral proteins to affect signal transmission and cell cycle [32].

In conclusion, this study provides evidence that *PPP2R5C* is a potential marker for metastasis and recurrence of OS, which may provide a suitable tumor microenvironment for metastasis by promoting TANs aggregation. However, there are several limitations in this study. First, because of the absence of the clinical characteristics of OS patients, we were not able to predict and compare the survival between metastatic OS and non-metastatic OS patients. Second, there are few studies on the correlation between these potential markers and TANs and OS, which means that their mechanism of action is unknown. Third, the rescue experiments in this study were incomplete, and the effect of *PPP2R5C* overexpression on OS cell lines was not verified. Fourth, we were not able to isolate TANs from the blood of patients with OS due to the lack of ethics approval. We used the OS cell lines U2-OS and MG63 for validation. Nevertheless, we will try to use TANs as material in future studies to explore the relationship between TANs and OS. Despite these limitations, *PPP2R5C* may be a potential target to modify the metastasis and recurrence of OS.

Conclusions

In this study, we found that TANs aggregation may promote OS metastasis. *PPP2R5C*, *PPP2R5E*, *YWHAG*, and *CREBBP* were highly expressed in human OS cell lines, U2-OS and MG63, in which *PPP2R5C* was found to reduce proliferation and migration and increase apoptosis of cancer cells by activating PI3K-AKT signaling pathway. *PPP2R5C* may be a potential target to decrease the metastasis and recurrence of OS.

Availability of Data and Materials

The data that support the findings of this study are available from the corresponding author upon reasonable request.

Author Contributions

ST and RC both conceived and designed the study and performed the bioinformatics analysis and experiments. ST collected the data and wrote the draft, and RC analyzed the data and defined the manuscript. Both authors contributed to the editorial changes in the manuscript. Both authors read and approved the final manuscript. Both authors have participated sufficiently in the work and agreed to be accountable for all aspects of the work.

Ethics Approval and Consent to Participate

Not applicable.

Acknowledgment

Not applicable.

Funding

This research was supported by the Chongqing Natural Science Foundation (No. 2022NSCQ-MSX3868) and Chongqing Yuzhong District Basic Research and Frontier Exploration Project (No. 20190139) from China.

Conflict of Interest

The authors declare no conflict of interest.

Supplementary Material

Supplementary material associated with this article can be found, in the online version, at https://doi.org/10.24976/Discov.Med.202335176.31.

References

[1] Moreno F, Cacciavillano W, Cipolla M, Coirini M, Streitenberger P, López Martí J, *et al*. Childhood osteosarcoma: Incidence and survival in Argentina. Report from the National Pediatric Cancer Registry, ROHA Network 2000-2013. Pediatric Blood & Cancer. 2017; 64: e26533.

[2] Cole S, Gianferante DM, Zhu B, Mirabello L. Osteosarcoma: A Surveillance, Epidemiology, and End Results program-based analysis from 1975 to 2017. Cancer. 2022; 128: 2107–2118.

[3] Song K, Song J, Lin K, Chen F, Ma X, Jiang J, *et al*. Survival analysis of patients with metastatic osteosarcoma: a Surveillance, Epidemiology, and End Results population-based study. International Orthopaedics. 2019; 43: 1983–1991.

[4] Petitprez F, Vano YA, Becht E, Giraldo NA, de Reyniès A, Sautès-Fridman C, *et al*. Transcriptomic analysis of the tumor microenvironment to guide prognosis and immunotherapies. Cancer Immunology, Immunotherapy: CII. 2018; 67: 981–988.

[5] Mikami S, Mizuno R, Kondo T, Shinohara N, Nonomura N, Ozono S, *et al*. Clinical significance of programmed death-1 and programmed death-ligand 1 expression in the tumor microenvironment of clear cell renal cell carcinoma. Cancer Science. 2019; 110: 1820–1828.

[6] Lecot P, Sarabi M, Pereira Abrantes M, Mussard J, Koenderman L, Caux C, *et al*. Neutrophil Heterogeneity in Cancer: From Biology to Therapies. Frontiers in Immunology. 2019; 10: 2155.

[7] Rubenich DS, Omizzollo N, Szczepański MJ, Reichert TE, Whiteside TL, Ludwig N, *et al*. Small extracellular vesicle-mediated bidirectional crosstalk between neutrophils and tumor cells. Cytokine & Growth Factor Reviews. 2021; 61: 16–26.

[8] Que H, Fu Q, Lan T, Tian X, Wei X. Tumor-associated neutrophils and neutrophil-targeted cancer therapies. Biochimica et Biophysica Acta. Reviews on Cancer. 2022; 1877: 188762.

[9] Khan S, Mittal S, McGee K, Alfaro-Munoz KD, Majd N, Balasubramaniyan V, *et al*. Role of Neutrophils and Myeloid-Derived Suppressor Cells in Glioma Progression and Treatment Resistance. International Journal of Molecular Sciences. 2020; 21: 1954.

[10] Hao Y, Hu P, Zhang J. Genomic analysis of the prognostic effect of tumor-associated neutrophil-related genes across 15 solid cancer types: an immune perspective. Annals of Translational Medicine. 2020; 8: 1507.

[11] Huang H, Zhang H, Onuma AE, Tsung A. Neutrophil Elastase and Neutrophil Extracellular Traps in the Tumor Microenvironment. Advances in Experimental Medicine and Biology. 2020; 1263: 13–23.

[12] Yoshihara K, Shahmoradgoli M, Martínez E, Vegesna R, Kim H, Torres-Garcia W, *et al*. Inferring tumour purity and stromal and immune cell admixture from expression data. Nature Communications. 2013; 4: 2612.

[13] Chen Y, Liu S, Shen Q, Zha X, Zheng H, Yang L, *et al*. Differential gene expression profiles of PPP2R5C-siRNA-treated malignant T cells. DNA and Cell Biology. 2013; 32: 573–581.

[14] Wang Y, Liang Y, Xu H, Zhang X, Mao T, Cui J, *et al*. Single-cell analysis of pancreatic ductal adenocarcinoma identifies a novel fibroblast subtype associated with poor prognosis but better immunotherapy response. Cell Discovery. 2021; 7: 36.

[15] Chen S, Zhang Q, Lu L, Xu C, Li J, Zha J, *et al*. Heterogeneity of neutrophils in cancer: one size does not fit all. Cancer Biology & Medicine. 2022; 19: 1629–1648.

[16] Zhang W, Shen Y, Huang H, Pan S, Jiang J, Chen W, *et al*. A Rosetta Stone for Breast Cancer: Prognostic Value and Dynamic Regulation of Neutrophil in Tumor Microenvironment. Frontiers in Immunology. 2020; 11: 1779.

[17] Wang X, Qiu L, Li Z, Wang XY, Yi H. Understanding the Multifaceted Role of Neutrophils in Cancer and Autoimmune Diseases. Frontiers in Immunology. 2018; 9: 2456.

[18] Bonecchi R, Mantovani A, Jaillon S. Chemokines as Regulators of Neutrophils: Focus on Tumors, Therapeutic Targeting, and Immunotherapy. Cancers. 2022; 14: 680.

[19] Raftopoulou S, Valadez-Cosmes P, Mihalic ZN, Schicho R, Kargl J. Tumor-Mediated Neutrophil Polarization and Therapeutic Implications. International Journal of Molecular Sciences. 2022; 23: 3218.

[20] Amin P, Awal S, Vigneron S, Roque S, Mechali F, Labbé JC, *et al*. PP2A-B55: substrates and regulators in the control of cellular functions. Oncogene. 2022; 41: 1–14.

[21] Lei X, Ma N, Du L, Liang Y, Zhang P, Han Y, *et al*. PP2A and tumor radiotherapy. Hereditas. 2020; 157: 36.

[22] El Taweel M, Gawdat RM, Abdelfattah R. Prognostic Impact of PPP2R5C Gene Expression in Adult Acute Myeloid Leukemia Patients with Normal Cytogenetics. Indian Journal of Hematology & Blood Transfusion. 2020; 36: 37–46.

[23] Zheng H, Chen Y, Chen S, Niu Y, Yang L, Li B, *et al*. Expression and distribution of PPP2R5C gene in leukemia. Journal of Hematology & Oncology. 2011; 4: 21.

[24] Baumgartner U, Berger F, Hashemi Gheinani A, Burgener SS, Monastyrskaya K, Vassella E. miR-19b enhances proliferation and apoptosis resistance via the EGFR signaling pathway by targeting PP2A and BIM in non-small cell lung cancer. Molecular Cancer. 2018; 17: 44.

[25] Dudek AM, van Kampen JGM, Witjes JA, Kiemeney LALM, Verhaegh GW. LINC00857 expression predicts and mediates the response to platinum-based chemotherapy in muscle-invasive bladder cancer. Cancer Medicine. 2018; 7: 3342–3350.

[26] Fan X, Cui L, Zeng Y, Song W, Gaur U, Yang M. 14-3-3 Proteins Are on the Crossroads of Cancer, Aging, and Age-Related Neurodegenerative Disease. International Journal of Molecular Sciences. 2019; 20: 3518.

[27] Wang J, Pan X, Li J, Zhao J. TXNDC9 knockdown inhibits lung adenocarcinoma progression by targeting YWHAG. Molecular Medicine Reports. 2022; 25: 203.

[28] Xu J, Wang J, He Z, Chen P, Jiang X, Chen Y, *et al*. LncRNA CERS6-AS1 promotes proliferation and metastasis through the upregulation of YWHAG and activation of ERK signaling in pancreatic cancer. Cell Death & Disease. 2021; 12: 648.

[29] Wang P, Deng Y, Fu X. MiR-509-5p suppresses the proliferation, migration, and invasion of non-small cell lung cancer by targeting YWHAG. Biochemical and Biophysical Research Communications. 2017; 482: 935–941.

[30] Mei J, Liu Y, Xu R, Hao L, Qin A, Chu C, *et al*. Characterization of the expression and prognostic value of 14-3-3 isoforms in breast cancer. Aging. 2020; 12: 19597–19617.

[31] Huang YH, Cai K, Xu PP, Wang L, Huang CX, Fang Y, *et al*. CREBBP/EP300 mutations promoted tumor progression in diffuse large B-cell lymphoma through altering tumor-associated macrophage polarization via FBXW7-NOTCH-CCL2/CSF1 axis. Signal Transduction and Targeted Therapy. 2021; 6: 10.

[32] Dyson HJ, Wright PE. Role of Intrinsic Protein Disorder in the Function and Interactions of the Transcriptional Coactivators CREB-binding Protein (CBP) and p300. The Journal of Biological Chemistry. 2016; 291: 6714–6722.